RSC Advances

PAPER

View Article Online
View Journal | View Issue

Cite this: *RSC Adv.*, 2021, **11**, 15410

Biomass-derived porous graphene for electrochemical sensing of dopamine†

Faisal Mahmood,[ab] Yisheng Sun[a] and Caixia Wan*[a]

Received 27th January 2021
Accepted 1st April 2021

DOI: 10.1039/d1ra00735a

rsc.li/rsc-advances

Cost-effective valorization of biomass into advanced carbon remains a challenge. Here we reported a facile and ultrafast laser writing technique to convert biomass into porous graphene for electrochemical sensing. Laser-induced graphene (LIG) was synthesized from a fully biomass-based film composed of kraft lignin (KL) and cellulose nanofibers (CNFs). The LIG-based electrode was applied to detect dopamine using cyclic voltammetry (CV) and differential pulse voltammetry (DPV) techniques. Dopamine with a concentration ranging from 5 to 40 μM was detected linearly, with a sensitivity of 4.39 μA μM^{-1} cm^{-2}. Our study eliminated the use of synthetic polymer for lignin-based film formation. It demonstrated the feasibility of using the film fully composed of biomass for LIG formation. Furthermore, derived LIG electrodes were shown to have high electrochemical sensing performance.

1. Introduction

Lignocellulosic biomass consisting primarily of cellulose, lignin, and hemicellulose is a promising feedstock for biofuels and bio-based products. Among the three major components, cellulose is the most abundant natural polymer making up 30–45% of lignocellulosic biomass, and hierarchal structures of cellulose microfibrils endow biomass with remarkable mechanical properties.[1] Lignin is the most abundantly available natural aromatic polymer providing mechanical support and protection to plants. Lignin can be readily separated from biomass *via* various pulping/pretreatment methods. Approximately 50 million tons of lignin are annually generated as a waste byproduct from pulp mills especially where kraft lignin is prevailing. However, most technical lignin is underutilized and ends up being burned as low quality solid fuel.[2] Therefore, researchers have invested great efforts to open new avenues to lignin valorization. To this end, upgrading lignin into advance carbon materials, such as graphene-based materials, has been proposed to be a promising approach for higher value-added utilization of lignin.

Graphene is a 2D sheet of sp^2 carbon atom bonded in a hexagonal honeycomb lattice and has gained tremendous interest worldwide since its discovery back to 2004. Due to its intriguing thermal, electrical, and mechanical properties, graphene is a multifunctional nanomaterial for various industrial applications.[3,4] There are several ways to fabricate graphene, such as micromechanical cleavage, liquid-phase exfoliation (LPE),[5] and chemical vapor deposition (CVD).[6] However, these techniques could be energy-intensive, tedious, and/or lengthy, which can hinder mass production of graphene-based materials. In contrast, direct laser writing (DLW) is a facile method for graphene fabrication that can address the drawbacks of the aforementioned techniques. It features a one-step, ultrafast, and chemical-free process for graphene formation by using a CO_2 laser that can even be found in a machine shop. More strikingly, DLW enables the formation of 3D interconnected carbon network with hierarchical structure (so-called laser-induced graphene (LIG)). Such unique structure together with intrinsic properties of graphene makes LIG a versatile platform nanomaterial for energy storage, catalysis, sensing, *etc.* For electrochemical sensing, LIG-based electrodes have been shown to detect a wide range of analytes (*e.g.*, biomarkers, neurotransmitters, proteins) as well as pathogens, with remarkable sensitivity and selectivity.[7–9]

DLW has been applied to a broad spectrum of substrates ranging from synthetic to natural polymers.[10–12] Despite substrate source, a precursor with aromaticity is generally favorable for LIG formation. This is exemplified by lignin that plays a key role in the induction of high-quality graphene from biomass-based substrates.[12–14] In contrast to lignin, cellulose as another major biomass constituent is not as readily inducible as lignin for LIG formation.[10,15] Based on prior studies, lignin dispersed in the form of a film or embedded into a matrix can be more properly and effectively lased.[10,12–14,16] A synthetic polymer (*e.g.*, PEO, PVA) can be used as a binder for the fabrication of lignin-based film.[13,14,17] Alternatively, cellulose can also be used as a natural binder for lignin-based film even if cellulose itself may not directly contribute to LIG formation under

[a]*Department of Biomedical, Biological, and Chemical Engineering, University of Missouri, Columbia 65211, USA. E-mail: wanca@missouri.edu; Fax: +1 573 884 5650; Tel: +1 573 884 7882*

[b]*Department of Energy Systems Engineering, University of Agriculture Faisalabad, Faisalabad 38000, Pakistan*

† Electronic supplementary information (ESI) available. See DOI: 10.1039/d1ra00735a

a suboptimal condition. However, a film fully based on lignin and nanocellulose has yet to been explored for LIG formation.

The main objective of this study was to explore biomass-based natural polymers for LIG production. A fully biomass-based film composed of cellulose nanofibers (CNFs) and kraft lignin (KL) was prepared. The effects of lignin content in the film and laser power on LIG were investigated using various characterization techniques. The characterized LIG was further evaluated for its performance as an electrochemical sensor for neurotransmitter (*i.e.*, dopamine).

2. Materials and methods

2.1. Materials

CNFs were purchased from The University of Maine Process Development Center (Orono, Maine). KL was kindly provided by Domtar Cooperation (Fort Mills, South Carolina). All the chemicals were purchased from Fisher Scientific (Waltham, MA) and used as received.

2.2. Preparation of CNF/KL film and LIG

The CNF/KL film was fabricated by mixing CNFs with KL at a mass ratio ranging from 1 : 2 to 1 : 5. Specially, 1 g of KL was first fully dissolved in 10 mL of 2 wt% NaOH solution followed by the addition of CNF at 0.2–0.5 g. The mixture was kept stirring until obtaining a homogeneous dispersion and then cast onto a plastic Petri dish (9 cm in diameter) for air drying. The air-dried film was peeled off from the Petri dish and cut into desired dimensions for DLW.

A CO_2 laser (10.6 μm, H-Series 2012 Desktop laser, Full Spectrum, Las Vegas, NV) was used for LIG production, which had a pulse duration of ~14 μs and a maximum power setting of 40 W. All the DLW tests were conducted under ambient condition, with a beam size of 100 μm at a 'z' distance of 2 mm, an image density of 1000 pulses per inch (PPI), and a scan rate of 20 cm s^{-1}. The laser power setting was adjusted to 30–90% of the maximum for DLW.

2.3. Electrode fabrication and electrochemical sensing

The electrode for electrochemical sensing was fabricated by using the LIG formed from the CNF/KL film. The LIG power was first scraped off from the film and then sonicated for 2 h in 4% (v/v) Nafion™ solution in water/ethanol mixture (3.8 : 1, v/v). The sonicated mixture was cast on a glassy carbon electrode and air dried prior to being used as a working electrode. As depicted in Fig. 1, a three-electrode system was applied to electrochemical sensing where an LIG-based electrode was used as a working electrode, Ag/AgCl as a reference electrode, and a graphite electrode as a counter electrode. A stock solution of dopamine with a concentration of 1 mM was prepared and diluted as needed using phosphate-buffered saline.

2.4. Characterization

Sheet resistance (R_s) of LIG was measured using a four-probe bridge resistivity system (Keithly 2400 Series SourceMeter®). The Raman spectra were acquired on a Renishaw inVia™ at a wavelength of 633 nm. Fourier transform infrared (FTIR) spectra were acquired on attenuated total reflectance Fourier transform infrared spectroscopy (ATR-FTIR) with a wavelength from 400 to 4000 cm^{-1}. Thermogravimetric analysis (TGA) was performed on a TA Instruments Q500 using nitrogen gas, with the temperature increasing at a rate of 5 °C min^{-1}. LIG embedded onto the CNF/KL film was characterized for R_s, Raman, and FTIR, while LIG scraped from the film was used for TGA.

The microstructure of LIG was analyzed by the FEI Quanta 600 FEG Environmental Scanning Electron Microscope (ESEM).

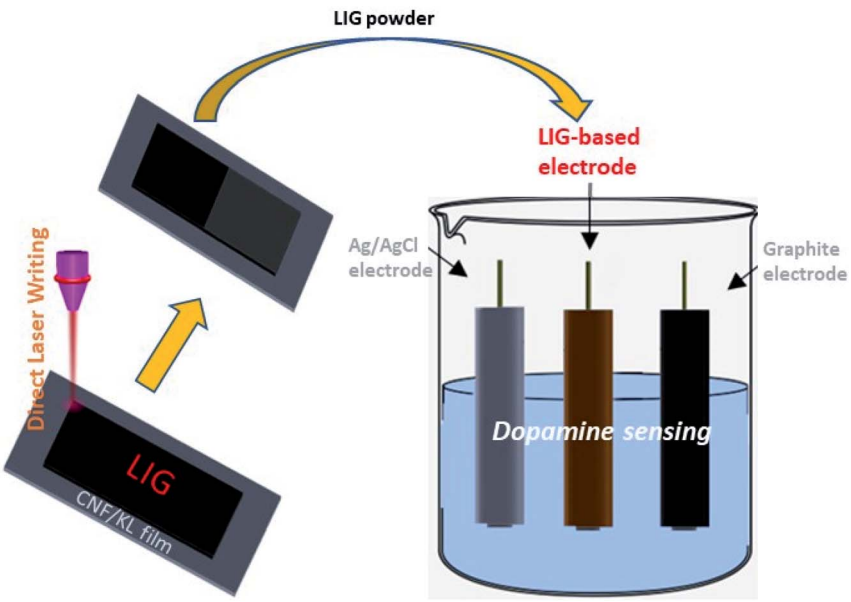

Fig. 1 Schematic illustration of LIG formation from a CNF/KL film and application of LIG-based electrode for electrochemical sensing.

SEM equipped with a Bruker Quantax 200 Silicon Drift Detector was operated at a 15 kV and 100 pA. The Energy-dispersive X-ray spectroscopy (EDS) was obtained by a Bruker Quantax 200 SDD-EDS detector. The data was processed in the ESPRIT 2 software suite. The spectra were collected for 3 min, which generated 3.6 M counts for each specified region. For both SEM and EDS, LIG embedded onto the film was placed on an SEM sample holder by applying an adhesive. Transmission Electron Microscopy (TEM) and high-resolution TEM (HRTEM) imaging were performed on a JEOL-2100FFEI Tecnai G2 F30 300 kV microscope. The sample was prepared by scraping off the CNF/KL LIG-70 and sonicated for 10 min in ethanol.

3. Results and discussion

3.1. Effects of lasing on the LIG formation from the CNF/KL film

We studied the effects of lasing on the LIG formation from the CNF/KL films. Fig. 2a depicts the R_s of LIG in response to laser power. In general, the LIG-derived from the film containing more lignin displayed the lower R_s. For the films containing lower lignin content (1 : 2–1 : 2.5), LIG formed from 50% laser power gave the lowest R_s. When the lignin content in the film increased, a higher power level (70%) led to lower R_s. The CNF/KL film with the highest mass ratio of 1 : 5 gave the LIG with the lowest R_s. Further increasing the mass ratio to 1 : 10 led to a film that was too brittle to be properly lased. Compared to the CNF/KL film, the neat CNF film did not yield LIG upon lasing. This could be attributed to single path lasing and protonated CNF. As reported in literature,[18] a neat CNF film was not well suited to LIG formation if lasing is applied to such film.[15] In general, cellulose is more recalcitrant to LIG formation than lignin as it is not structurally favorable for graphene formation and requires more intermediate steps toward graphitization.[10] Thus, it can be inferred that lignin in the CNF/KL film should play a precursor role in LIG formation.

The effect of laser power on LIG properties was further investigated using Raman Spectroscopy. As depicted in Fig. 2b, there are three characteristic peaks observed with LIG: a D peak at ~1350 cm^{-1} associated with defects and bending of sp^2 carbon bonds, a G peak at ~1580 cm^{-1} from first-order Raman band of all sp^2 hybridized carbon, and a 2D peak from second-order zone-boundary phonons.[19] It was found that 30% power led to low-quality graphitic carbon as reflected by the presence of broad D and G peaks only on the carbonized film. When the laser power was increased to 70%, the intensity of D peak decreased while those of both G and 2D peaks increased, indicating the formation of higher quality graphitic carbon. Correspondingly, the I_G/I_D ratio increased upon the change in laser power from 30% to 70%. A higher I_G/I_D ratio suggests a higher degree of graphitization.[19] Interestingly, the CNF/KL film gave LIG with less defects as evidenced by relatively suppressed D peaks compared to biomass-/lignin-based LIG reported in prior studies.[10,13,14] Elevating laser power to 80% or above resulted in

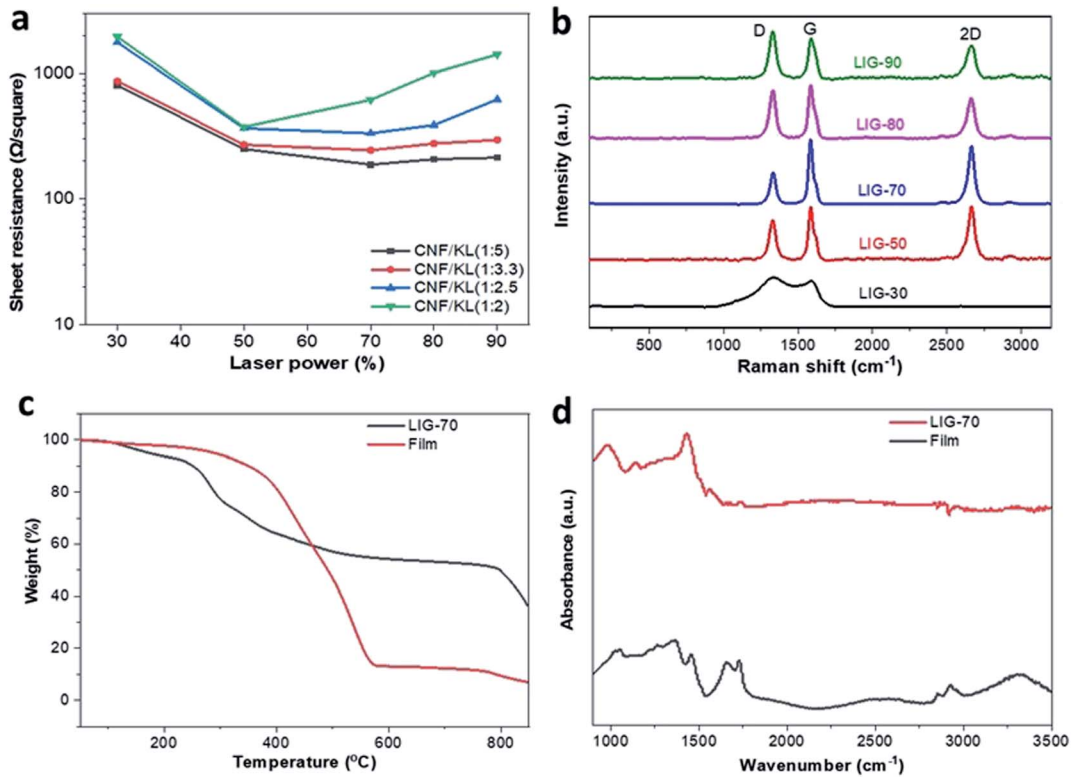

Fig. 2 Characterization of LIG. (a) Sheet resistance (R_s) of LIG derived from the CNF/KL films at different laser power. (b) Raman spectra of LIG (1 : 5) obtained at different laser power. (c) TGA analysis of LIG-70 (1 : 5) and pristine film. (d) FTIR analysis of LIG-70 (1 : 5) and original film. LIG-70 (1 : 5) represents LIG derived from the CNF/KL (1 : 5) film at 70% laser power.

a decrease in I_G/I_D ratio, which can be attributed to the partial oxidation of LIG as the lasing was performed at atmosphere under ambient condition. Nevertheless, when laser was applied at an optimal power (*i.e.*, 70%), high quality fewer-layered graphene with a crystalline structure was formed from the CNF/KL film.

LIG formed at 70% laser power from the CNF/KL (1 : 5) film (denoted as LIG-70(1 : 5)) was analyzed for thermal degradation, with the pristine film (*i.e.*, non-carbonized) as a control. Fig. 2c shows the thermal degradation profiles of both samples. Before reaching a temperature of 600 °C, the pristine film lost ~90% of its initial mass, whereas LIG retained more than 50% of its mass. The thermal degradation profile confirmed that a higher degree of graphitization occurred at 70% laser power as reflected by significantly improved thermal stablity of LIG. Graphitization of the CNF/KL film was further corroborated by FTIR analysis. As depicted in Fig. 2d, the hydroxyl groups (3400 cm^{-1}) disappeared along with other characteristics peaks after lasing.[12,20] The peaks of LIG arising at near 1000 and 1400 cm^{-1} can be associated with the stretching of C–O–C groups and the vibrations of carboxylic groups, respectively. The presence of oxygen-binding carbon can be attributed to oxidation of highly oxidized CNF/KL film substrate when lasing in air. The presence of oxygen in the LIG was also verified by EDS as depicted in ESI.†

LIG-70(1 : 5) was also examined for morphology and microstructure by SEM. Fig. 3a and b displayed the porous 3D structure of the obtained LIG. At higher magnifications, we observed that the surface consists of a network of randomly distributed mesopores and macropores (Fig. S1†). This 3D network of porous carbon would be beneficial for various applications such as energy storage and electrochemical sensing. It has been reported that electrochemical response can be enhanced by an interconnected 3D carbon network of graphene, as it has high specific surface area and electrically conductive pathways facilitating efficient charge transfer and mass transfer.[21–25] Various bright spots were also noticed across the surface of LIG by SEM imaging (Fig. S2a†). These bright spots were analyzed *via* EDS and compared to the surface with no bright spots. EDS was performed on two regions as shown in Fig. S2a and b.† The normal region is highlighted (Fig. S2a†) and a bright spot is represented by a square (Fig. S2b†). The peak of carbon was normalized to get a comprehensive comparison. As depicted in ESI,† carbon was consistent at both spots, whereas oxygen and sodium had slightly higher concentrations. Sodium originated from NaOH that was added

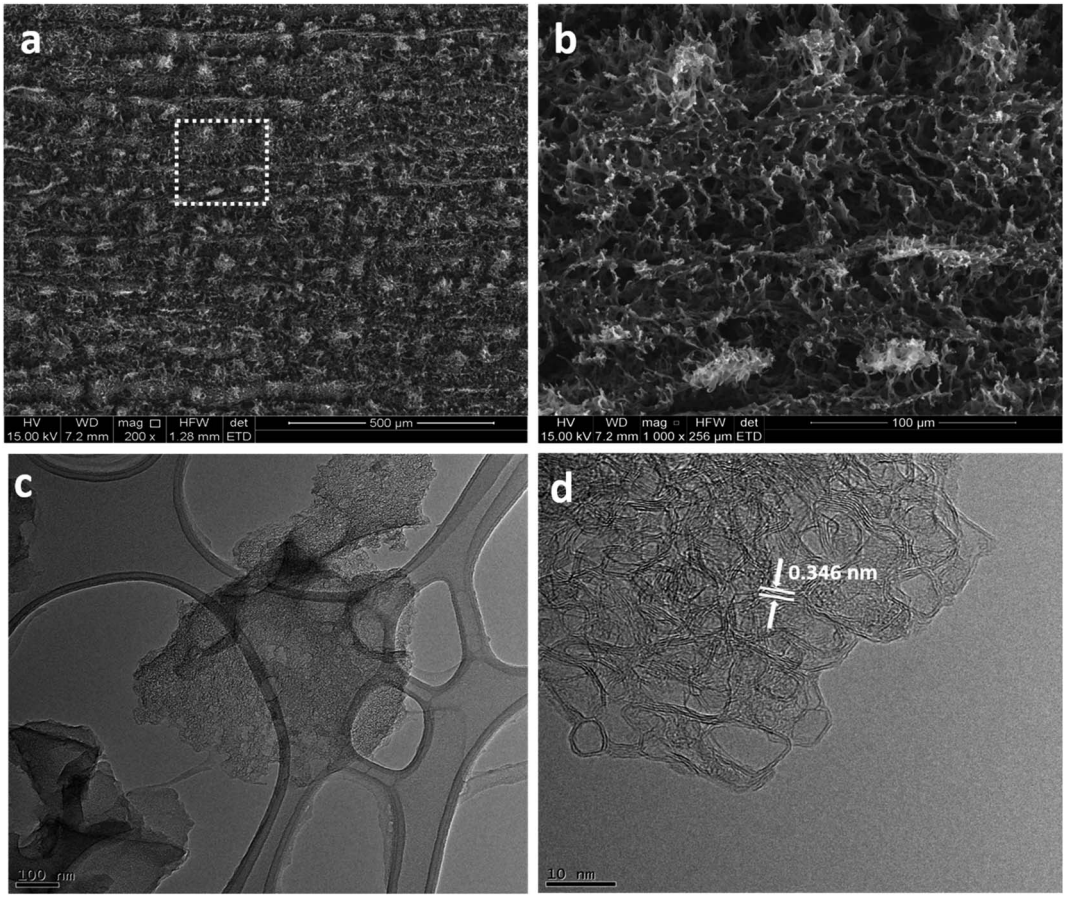

Fig. 3 Morphology and microstructure of LIG-70 (1 : 5). (a) SEM images of LIG-70 (1 : 5), with a scale bar of 500 µm. (b) SEM images of LIG-70 (1 : 5), corresponding to the white square in (a) at higher magnification with a scale bar of 100 µm. (c) TEM image, with a scale bar of 100 nm. (d) HRTEM image representing fringe-like structures, with a scale bar of 10 nm.

to dissolve the KL for the fabrication of pristine CNF/KL film, which could promote the growth of carbonaceous materials and further graphitization.[15,26] LIG-70(1 : 5) was further examined for ultrastructure by HRTEM (Fig. 3c and d). Fig. 3d reveals fringe-like structures that can also be found in LIG derived from other precursors.[11,27] Such fringe-like patterns are exposed edges of graphene layers, and their formation can be attributed to the thermal expansion during laser ablation.[11] The average spacing of 0.346 nm was observed, which corresponds to spacing between neighboring planes (002) in graphitic carbon (Fig. 3d).

Overall, characterization results prove that the CNF/KL film is a suitable substrate for the formation of few-layered graphene at a proper laser power. A porous 3D network of graphene with ample defect-rich boundaries demonstrated electrochemical sensing with high performance as discussed below.

3.2. Electrochemical sensing of dopamine

Using LIG-70(1 : 5) as an active electric material, we fabricated the electrode for dopamine sensing and explored the transport characteristics of dopamine *via* cyclic voltammetry (CV). Fig. 4a depicts CV recorded at 100 mV s^{-1} for sensing dopamine with a concentration of 1 mM. Compared to the control electrode (*i.e.*, glass carbon electrode only), LIG electrode showed significantly different performance. Specifically, the performance of LIG electrode was 4–5 times that of the glassy carbon electrode. This indicates that the 3D carbon network of the as-obtained LIG plays a crucial role in dopamine sensing. The performance of the LIG-applied electrode was further examined by varying the scan rate and keeping the concentration of dopamine constant at 1 mM. Fig. 4b displays the change in both anodic and cathodal peak currents as the scan rate is increased from 10 to 100 mV s^{-1}. With the increase of scan rate, the anodic (I_{pa}) and cathodic (I_{pc}) peaks not only increased but also shifted toward the positive and negative potentials, respectively. The peaks confirm that the reaction is quasi-reversible in response to the increase in current density (Fig. 4c).[28]

Differential Pulse Voltammetry (DPV) curves for dopamine sensing are depicted in Fig. 4d & e. A typical DPV curve is shown in Fig. 4d when a glassy carbon electrode was used as a working electrode to sense dopamine. Such control electrode shows a much lower detection capability when compared to the LIG-applied electrode (Fig. 3d *vs.* e). Oxidation current for the LIG-applied electrode also increased linearly with an increase in the dopamine concentration from 5 to 40 μM (R^2 = 0.995) (Fig. 4f). The DPV analysis suggests that the as-obtained LIG is capable of detecting dopamine with a sensitivity of 4.39 μA μM^{-1} cm^{-2}. The lowest detection limit was found to be 3.4 μM but out of linear range. While such limit is not impressively low compared to prior studies based on functionated LIG electrodes (*e.g.*, Pt deposited, Pt-AU deposited, PEDOT functionalized),[28–30] the DPV analysis suggests great potential for using derived LIG for dopamine sensing. The future study would be extended to

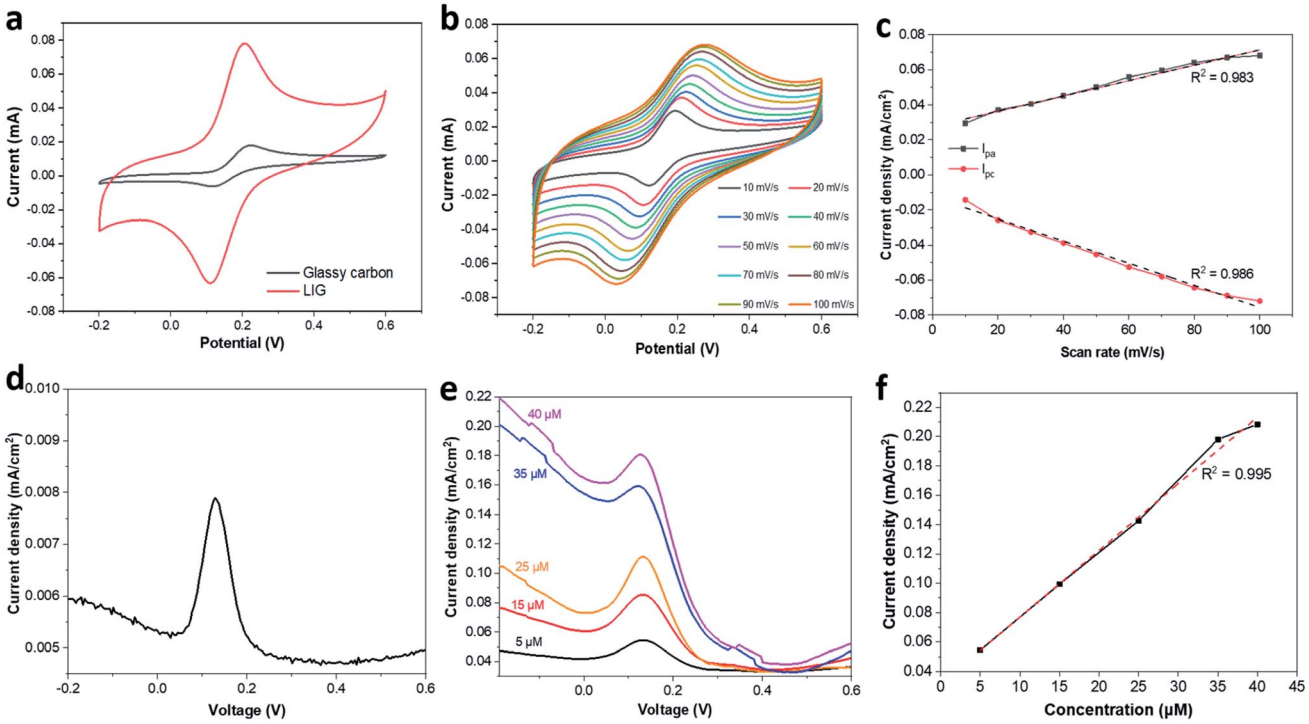

Fig. 4 Electrochemical sensing performance of LIG-based electrode. (a) Comparison of glassy carbon electrode with and without LIG. (b) CV analysis of LIG-based electrode at different scan rates. (c) Correlation between current density and scan rate. (d) DPV curve for glassy carbon electrode only sensing 5 μM dopamine solution. (e) DPV curves for LIG-based electrode sensing 5–40 μM dopamine solution. (f) Correlation between current density and dopamine sensing. LIG-70 (1 : 5) derived from the CNF/KL (1 : 5) film at 70% power was used for LIG-based electrode.

functionalization of the proposed biomass-derived LIG for ultrasensitive detection of dopamine and other biomolecules.

4. Conclusions

A facile technique was developed to produce LIG from a fully biomass-based film composed of CNFs and KL. The obtained LIG presented a 3D interconnected porous graphene network with defect-rich boundaries. Lignin played a precursor role in LIG formation, and the film containing more lignin was more favorable for LIG formation. Laser power was found to have a significant effect on LIG quality. Derived LIG applied to a glassy carbon electrode made the hybrid electrode exhibiting outstanding performance in dopamine sensing, which was 4–5 times high that of the unmodified glassy carbon electrode. A strong linear correlation between oxidation current and dopamine concentration was observed with the LIG-based electrode. Overall, this work demonstrated that LIG electrode can be facilely fabricated from naturally occurring polymers and used for electrochemical sensing with impressive performance. Our study would also open a new revenue to biomass/lignin valorization toward high-value graphene-based materials for biosensing application.

Conflicts of interest

The authors declare that they have no competing interests.

Acknowledgements

This work is supported by the National Science Foundation (Grant No. 1933861). The authors also thank the support from the University of Missouri Electron Microscopy Core facility.

References

1 L. J. Gibson, *J. R. Soc., Interface*, 2012, **9**, 2749–2766.
2 T. Aro and P. Fatehi, *ChemSusChem*, 2017, **10**, 1861–1877.
3 A. K. Geim, *Science*, 2009, **324**, 1530–1534.
4 Y. Xie, C. Zhang, X. He, T. White, J. D. Demaree, M. Griep and J. Lin, *J. Power Sources*, 2018, **397**, 37–43.
5 S.-H. Lee, J. H. Kim and J.-R. Yoon, *Sci. Rep.*, 2018, **8**, 8179.
6 J. Li, G. Wang, H. Geng, H. Zhu, M. Zhang, Z. Di, X. Liu, P. K. Chu and X. Wang, *ACS Appl. Mater. Interfaces*, 2015, **7**, 19876–19881.
7 L. Huang, J. Su, Y. Song and R. Ye, *Nano-Micro Lett.*, 2020, **12**, 157.
8 A. Ghanam, A. A. Lahcen, T. Beduk, H. N. Alshareef, A. Amine and K. N. Salama, *Biosens. Bioelectron.*, 2020, **168**, 112509.
9 C. Zhang, Y. Xie, C. Zhang and J. Lin, *Carbon*, 2019, **153**, 585–591.
10 Y. Chyan, R. Ye, Y. Li, S. P. Singh, C. J. Arnusch and J. M. Tour, *ACS Nano*, 2018, **12**, 2176–2183.
11 J. Lin, Z. Peng, Y. Liu, F. Ruiz-Zepeda, R. Ye, E. L. G. Samuel, M. J. Yacaman, B. I. Yakobson and J. M. Tour, *Nat. Commun.*, 2014, **5**, 5714.
12 R. Q. Ye, Y. Chyan, J. B. Zhang, Y. L. Li, X. Han, C. Kittrell and J. M. Tour, *Adv. Mater.*, 2017, **29**, 1702211.
13 F. Mahmood, C. Zhang, Y. Xie, D. Stalla, J. Lin and C. Wan, *RSC Adv.*, 2019, **9**, 22713–22720.
14 F. Mahmood, H. Zhang, J. Lin and C. Wan, *ACS Omega*, 2020, **5**, 14611–14618.
15 S. Lee and S. Jeon, *ACS Sustainable Chem. Eng.*, 2018, **7**, 2270–2275.
16 S. Wang, Y. Yu, S. Luo, X. Cheng, G. Feng, Y. Zhang, Z. Wu, G. Compagnini, J. Pooran and A. Hu, *Appl. Phys. Lett.*, 2019, **115**, 083904.
17 W. L. Zhang, Y. J. Lei, F. W. Ming, Q. Jiang, P. M. F. J. Costa and H. N. Alshareef, *Adv. Energy Mater.*, 2018, **8**, 1801840.
18 S. Lee and S. Jeon, *ACS Sustainable Chem. Eng.*, 2019, **7**, 2270–2275.
19 A. C. Ferrari, J. C. Meyer, V. Scardaci, C. Casiraghi, M. Lazzeri, F. Mauri, S. Piscanec, D. Jiang, K. S. Novoselov, S. Roth and A. K. Geim, *Appl. Phys. Lett.*, 2006, **97**, 187401.
20 M. M. Gudarzi and F. J. E. P. L. Sharif, *eXPRESS Polym. Lett.*, 2012, **6**, 1017–1031.
21 X. Dong, X. Wang, L. Wang, H. Song, H. Zhang, W. Huang and P. Chen, *ACS Appl. Mater. Interfaces*, 2012, **4**, 3129–3133.
22 Z.-S. Wu, Y. Sun, Y.-Z. Tan, S. Yang, X. Feng and K. Müllen, *J. Am. Chem. Soc.*, 2012, **134**, 19532–19535.
23 N. Li, Q. Zhang, S. Gao, Q. Song, R. Huang, L. Wang, L. Liu, J. Dai, M. Tang and G. Cheng, *Sci. Rep.*, 2013, **3**, 1604.
24 M. Wu, S. Meng, Q. Wang, W. Si, W. Huang and X. Dong, *ACS Appl. Mater. Interfaces*, 2015, **7**, 21089–21094.
25 H.-J. Qiu, Y. Guan, P. Luo and Y. Wang, *Biosens. Bioelectron.*, 2017, **89**, 85–95.
26 R. Shi, L. Tan, L. Zong, Q. Ji, X. Li, K. Zhang, L. Cheng and Y. Xia, *Carbohydr. Polym.*, 2017, **157**, 1594–1603.
27 R. Ye, D. K. James and J. M. Tour, *Acc. Chem. Res.*, 2018, **51**, 1609–1620.
28 P. Nayak, N. Kurra, C. Xia and H. N. Alshareef, *Adv. Electron. Mater.*, 2016, **2**, 1600185.
29 G. Xu, Z. A. Jarjes, V. Desprez, P. A. Kilmartin and J. Travas-Sejdic, *Biosens. Bioelectron.*, 2018, **107**, 184–191.
30 X. Hui, X. Xuan, J. Kim and J. Y. Park, *Electrochim. Acta*, 2019, **328**, 135066.